Enhancing the MA-free mixed halide perovskite efficiency and stability through bi-solvent engineering approach

Sofia A. Djouse-Ivanina, Atyom V. Novikov, Piotr Griscenco, Ilya N. Krupatin, Marina M. Tepliakova, Ilya E. Kuznetsov, Alexander V. Akkuratov, Sergey Yu. Luchkin, and Olga R. Parfenova *

Cite this article as: Sofia A. Djouse-Ivanina, *et.al*. Enhancing the MA-free mixed halide perovskite efficiency and stability through bi-solvent engineering approach. *Light: Advanced Manufacturing* accepted article preview 28 April 2025; doi: 10.37188/lam.2025.039

Received 19 June 2024; Revised 24 April 2025; Accepted 24 April 2025; Accepted article preview online 28 April 2025

Enhancing the MA-free mixed halide perovskite efficiency and stability through bi-solvent engineering approach

Sofia A. Djouse-Ivanina[1], Atyom V. Novikov[1], Piotr Griscenco[1], Ilya N. Krupatin[2], Marina M. Tepliakova[1], Ilya E. Kuznetsov[3], Alexander V. Akkuratov[3], Sergey Yu. Luchkin[1], and Olga R. Parfenova[1,*]

[1] Center for Energy Science and Technology, Skolkovo Institute of Science and Bolshoy Boulevard, 30, p.1, Moscow 121205, Russia.

[2] Advanced Imaging Core Facility, Skolkovo Institute of Science and Technology, Bolshoy Boulevard, 30, p.1, Moscow 121205, Russia.

[3] Federal Research Center of Problems of Chemical Physics and Medicinal Chemistry Russian Academy of Sciences (FRC PCPMC RAS), Academician Semenov avenue 1, Chernogolovka, 142432, Russia

O.Iamilova@skoltech.ru

Abstract

Perovskite photovoltaics upholds the most prominent position in the field of tandem technology development. In this aspect, the creation of perovskite material with suitable bandgap (≥ 1.65 eV) is necessary. And in order to achieve the best device characteristics, the high-quality film formation is crucial. To get a high-quality film, the solvent engineering approach stays at the forefront. However, although the solvent engineering was well discussed for such conventional material as $MAPbI_3$, the field of wide bandgap perovskite materials is still lacking in this area. This paper presents the solvent engineering approach to improve the efficiency and stability of the conventional wide bandgap perovskite material $Cs_{0.17}FA_{0.83}PbI_{1.8}Br_{1.2}$. Here we utilize several solvents such as traditional N,N-dimethylformamide, dimethyl sulfoxide, N-methyl-2-pyrrolidone and acetonitrile. It was demonstrated that implication of any binary DMF-

X solvent improves the solar cell efficiency compared to the pure DMF solution, but the ratio of the X solvent is unique for every X and the foundation for the X influence is also unique. The addition of 2.4 M of DMSO is considered the best to improve the stability and efficiency of laboratory devices, however implementation of AcN allowed to produce 25 cm^2 mini-modules with the PCE reaching 10%.

Keywords: Perovskite photovoltaics, Wide bandgap perovskite, Solvent engineering, Large-area perovskite modules

Introduction

Nowadays, perovskite photovoltaics is a technology that needs no introduction. Unprecedented rapid increase in efficiency from 3.8% up to 26.1% for single-junction solar cells in less than 15 years proved the bright future of the technology.[1,2] However, according to the recent market research, the most promising implementations can be achieved in the areas of indoor photovoltaics, semi-transparent devices and multi-junction solar cells.[3-5] Accordingly, the development of so-called wide bandgap (WBG) perovskite materials with $E_g \geq 1.7$ eV becomes the key to the mentioned market areas. Significant progress was made in the field of WBG perovskite material design, where majority of the state-of-the-art WBG perovskite systems contain a mixture of ions. [6-9] The precise adjustment of the bandgap is achieved by altering the ratios of the both A cations and X anions in the ABX_3 structure and such mixed-ion perovskites have superior performance and stabilized efficiency.[10] Some reports state that FA^+ based WBG perovskites possess higher stability than MA^+ based ones.[11] And introducing from y = 0.1 to y = 0.3 Cs^+ increases the crystalline quality, carrier lifetime and mobility of $FA_{1-y}Cs_yPbI_xBr_{3-x}$ perovskites. [12]

But despite the significant progress in the chemical design of WBG perovskite materials, there are still some issues that need to be addressed. Photoinduced phase segregation often occurs upon illumination: halides separate into I-rich lower bandgap regions and Br-rich higher bandgap regions. The lower bandgap regions act as recombination centers for photogenerated charge carriers, causing voltage losses.[13] And Br-dominated inhomogeneities are formed in the perovskite structure, which leads to

the poor film morphology with large amount of pinholes.[14] Grain boundaries and defects limit the mobility of the charge carriers and serve as recombination sites.[15] Overall, the defect concentration and phase homogeneity should be improved to enhance operational stability of the WBG perovskite material. Major strategies employed to achieve these goals include compositional engineering, [16,17] surface passivation, [18-20] solvent engineering. [21,22]

As we already mentioned, compositional engineering of WBG perovskites is highly developed topic. Same can be said about the passivation methods. There are approaches for directly address certain defects by certain passivators, as well as overall passivation for stability or device parameters improvement. And also the approach for the development of self-assembled monolayers. Unfortunately, there are not many publications dedicated to the solvent engineering method for WBG perovskites. Classic materials, namely, methylammonium lead iodide $MAPbI_3$ were thoroughly investigated, and a number of successful methods including one- and two-step spin coating, antisolvent-free and solvent-free methods were developed.[23-25] Limited solubility of perovskite precursors in a single solvent leaded to the recommendation to apply mixed-solvent systems. Furthermore, the optimal ratio of additional DMSO solvent was found to be within the 20-40 vol. % range.[26] Also, a number of publications investigated the wet film formation processes for such materials as $FAPbBr_3$, $FAPbI_3$ and $CsPbI_3$.[27-29] Xu et al. implied NMP/DMF solvent system for $MA_{0.05}Cs_{0.12}FA_{0.83}Pb(I_{0.6}Br_{0.4})_3$ perovskite and obtained higher efficiency relative to the DMSO/DMF solvent system.[30] Despite that, the solvent optimization for complex multi-cation and multi-anion materials is still in a nascent stage. Even for the materials with the same chemical formula, there can be several approaches for film deposition. For example, in various works, wide bandgap perovskite material $Cs_{0.17}FA_{0.83}PbI_{1.8}Br_{1.2}$ was deposited from pure DMF,[31] DMF:DMSO 9:1,[32] DMF:DMSO 8:2,[33] and pure DMSO solvents,[34] leading to the various device characteristics.

Here we present the first attempt to understand the influence of various binary solvents on the $Cs_{0.17}FA_{0.83}PbI_{1.8}Br_{1.2}$ wide bandgap perovskite film formation. We've chosen this MA-free based perovskite first introduced by McMeekin et al.[31] due to its optimal bandgap around 1.75 eV suitable for both indoor and multi-junction photovoltaics. In this work we implemented simple one-step spin-coating method with

antisolvent application for its simplicity, reproducibility and the possibility to test various solvents in similar deposition conditions. During the investigation we considered traditional perovskite solvents N,N-dimethylformamide (DMF) and dimethyl sulfoxide (DMSO), also N-Methyl-2-pyrrolidone (NMP) and acetonitrile (AcN). It was demonstrated that implication of any binary DMF-X solvent improves the solar cell efficiency compared to the pure DMF solution. We also produced large area (25 cm^2) modules with the best binary solvent combinations and demonstrated that despite the best efficiency in laboratory devices was achieved for DMF-DMSO processed solar cells, the best efficiency for modules was obtained for DMF-AcN devices.

Results

For all of the following experiments we used a pure DMF solution of $Cs_{0.17}FA_{0.83}PbI_{1.8}Br_{1.2}$ with concentration of 1.2 M as a reference system. To investigate the influence of additional solvent we partially substituted DMF with either DMSO, NMP or AcN to keep the perovskite concentration constant, while concentration of additional solvent was set as 0 M (pure DMF references), 0.48 M, 0.72 M, 1.2 M, 2.4 M and for DMSO also 2.8 M. These values were chosen as corresponding to the total concentration of ions in solution: $C(Br^-)$ = 0.48 M, $C(I^-)$ = 0.72 M, $C(Br^-) + C(I^-)$ = $C(Pb^{2+})$ = 1.2 M, $C(Br^-) + C(I^-) + C(Pb^{2+})$ = 2.4 M. Concentration of 2.8 M of DMSO is equal to 20 Vol%, which is one of the most often used ratios in DMF-DMSO binary solvent systems.

Figure 1 demonstrates the n-i-p device architecture (ITO/SnO_2/PCBA/perovskite/PTAA/VO_x/Al) and influence of additional solvent concentration on its parameters: PCE, V_{OC}, J_{SC} and FF. Examples of *J*-V curves, EQE spectra and PCE statistics for the reference and best additional solvent concentrations can be found in Supplement (Fig. S1). Pure DMF reference system demonstrated efficiency around 11-12%, while partial substitution of solvent increased the efficiency up to 12-13.5% (2.4 M DMSO), 12-13% (0.72 M NMP) and 11.5-12.5% (1.2 M AcN). We can state that AcN addition mostly influenced the FF of the device, increasing it from 60% to 67%. NMP addition increased device J_{SC} from 17.3 up to 18.3 mA/cm^2. And DMSO influenced both J_{SC} (from 17.3 up to 18.5 mA/cm^2) and FF (from 60 up to 67%), leading to the highest increase in PCE. This implicates the different reasons

behind the solvents influence on device performance. To determine these reasons further investigations were performed mostly for four solvent compositions: pure DMF as reference, AcN 1.2 M, NMP 0.72 M and DMSO 2.4 M as the best representatives for each binary combination.

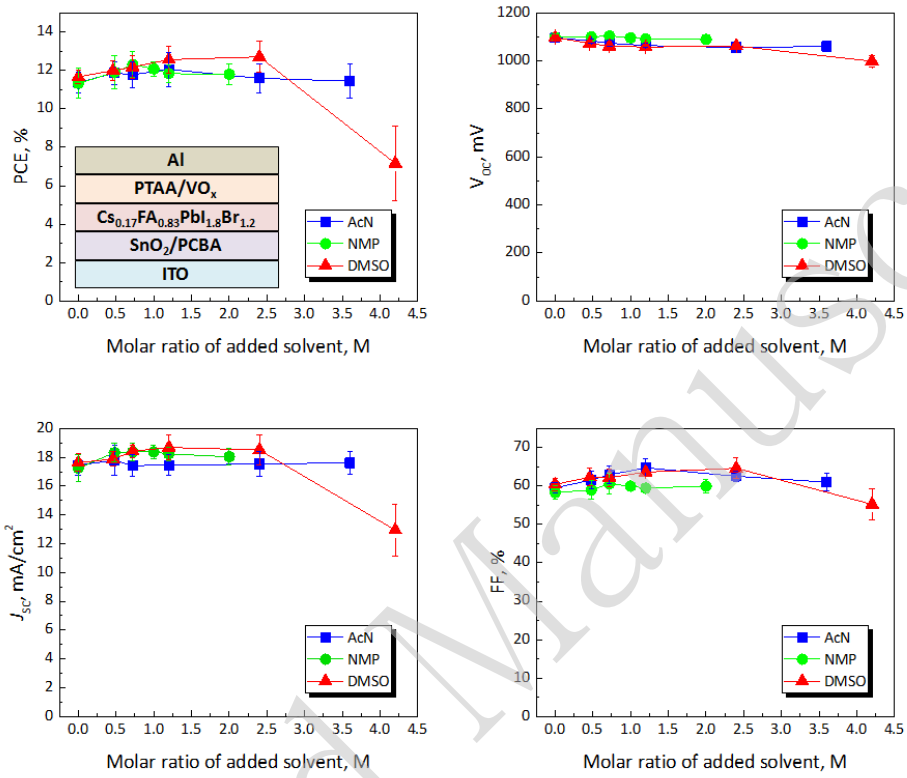

Figure 1. Influence of DMF solvent partial substitution with AcN, NMP or DMSO on solar cell parameters. Here presented all main solar cell parameters of solar cells: PCE, V_{OC}, J_{SC} and FF. Inside the PCE figure, the device architecture for this test is presented.

UV-Vis spectra (Fig. 2a) demonstrated slight increase of intensity for AcN 1.2 M and NMP 0.72 M perovskite films deposited on glass substrate compared to the pure DMF, while DMSO films demonstrated the highest absorption. This effect is most likely related to the increase in thickness of DMF-DMSO film, which is expected because DMSO has highest viscosity and boiling point among all presented solvents. The broad wave in the near-IR on absorption spectra is related to the interference of light reflected from both sides of the perovskite layer. SSPL from the same samples revealed that only DMSO addition increased the PL intensity (Fig. 2b). Time-resolved photoluminescence (TRPL) was used to determine the relative defect density in different samples, because the decrease in charge carrier lifetimes is reflected in a fast PL decay.[35] In Supplement (Fig. S2) the TRPL profiles with different solvents are

presented. The shape of the TRPL profiles depends on the rate of competitive recombination processes: fast trap-assisted recombination (non-radiative) and slow bimolecular recombination (radiative).[36,37] Therefore, the TRPL profiles for perovskite materials are usually fitted with exponential decay function:

$$N(t) = Ae^{\frac{-t}{\tau}} + \mathrm{C}$$

where A is PL decay amplitude, t is the decay time, τ – time of average recombination decay, C is a constant characterizing electron noise and diffuse light scattering background. Dependence of the average charge carrier lifetimes from the additional solvent concentration is shown in Fig. 2c. Average charge carrier lifetimes increase with any solvent addition. It is also noticeable that the shape of τ dependency resembles that of PCE dependency on additional solvents molar concentration: peak at 1.2 M for AcN, at 0.75 M for NMP and at 2.4 M for DMSO. Therefore, it is possible that improvement of device performance is related to the decreased defect density in WBG perovskite.

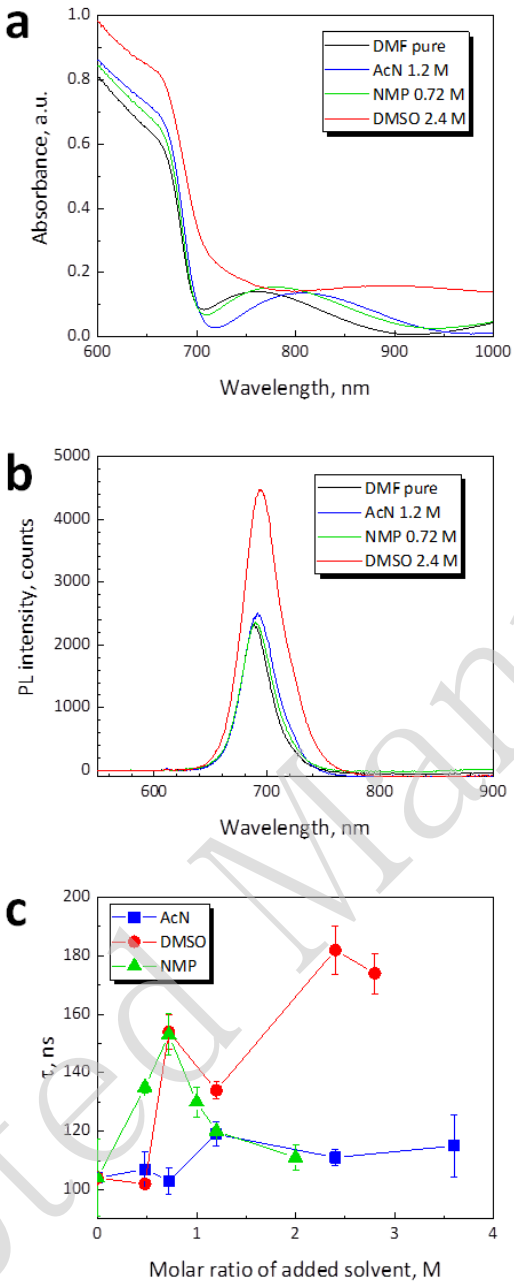

Figure 2. UV-Vis (a) and PL (b) spectra of perovskite films on glass substrates processed from different solution compositions. Influence of additional solvent concentration on the average lifetime of charge carriers τ calculated from the TRPL data (c).

The most significant changes in device basic parameters were observed in XRD spectra (Fig. 3a), where intensity increased for both AcN 1.2 M and NMP 0.72 M, while addition of DMSO inverted the intensity of peaks, making 20.3° and 32.3° dominant. This fact leads to the assumption that addition of NMP and AcN increases the grain size in perovskite film, while DMSO additionally changes the occupancy of crystallographic positions. The whole effect of XRD change depending on additional

solvent concentration can be observed in Supplement (Fig. S3).

AFM data confirmed the assumption of grain size growth (Fig. 3b), but we additionally performed SEM measurements from the film surface to confirm this (Supplement Fig. S4). AFM also revealed the improvements in perovskite film quality, as numerous defects visible for flat DMF films disappear for AcN 1.2 M and NMP 0.72 M films. The surface of the perovskite films with AcN addition remains flat up to 3.6 M of AcN added (Supplement Fig. S5). But only 1.2 M AcN samples demonstrated the grain size growth compared to the reference. Similar effect was observed for NMP addition up to 0.72 M. Further addition of NMP leaded to the formation of grain clusters (Supplement Fig. S5), which probably caused the further observed increase of XRD intensity, but decreased the average charge carrier lifetime and device PCE.

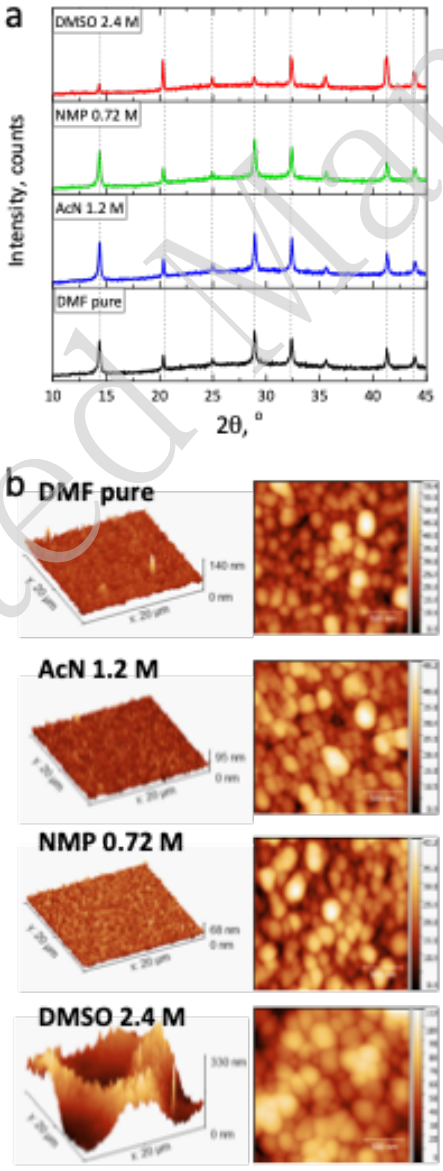

Figure 3. XRD spectra for perovskite films on glass substrates processed from different solution compositions (a). 3D AFM profiles for 20x20 μm scan area and 2D AFM profiles for 2x2 μm scan areas, perovskite films on glass substrates processed from different solution compositions (b).

With the DMSO introduction, films surface becomes more and more uneven, forming hills and valleys and becoming "wrinkled" (Fig. 3b, Supplement Fig. S5). Increase of DMSO concentration makes "wrinkles" larger and deeper. Wrinkled morphology is typical for mixed ion perovskites, and it appears due to relaxation of internal stresses during crystallization caused by misfits in ion sizes (e.g. the size of Br^- and I^- is 1.96 and 2.22 Å, respectively).[14] Wrinkles and folds in the surface effectively localize and trap light, which greatly improves light harvesting capabilities in optoelectronics.[38] Same effect is implemented in traditional structured silicon wafers for effective light harvesting in solar cells. That means that high J_{SC} for DMSO devices may be additionally attributed to their morphology. Simultaneously, "wrinkles" influence the film absorbance, as the light trapping increases the interference, leading to the lift in the UV-Vis baseline.

AFM method also allowed us to check the assumption of increasing of the film thickness, related to the additional solvents. Thickness of pure DMF films was confirmed at 350±10 nm. Addition of 1.2 M AcN or 0.72 M NMP did not lead to changes in the film thickness. However, DMSO 2.4 M films demonstrated the variation of thickness parameters because of "wrinkled" morphology from 300 nm up to 390 nm.

To get a deep insight into the influence of solvents on defect state in complete devices, we performed a series of investigations: Suns-V_{OC}, SCLC and Impedance spectroscopy (Fig. 4a-d). Impedance spectroscopy and Suns-V_{OC} were measured from the mentioned earlier device architecture ITO/SnO_2/PCBA/perovskite/PTAA/VO_x/Al, while for SCLC measurement we used electron-only configuration ITO/SnO_2/PCBA/perovskite/PCBM/BCP/Mg/Al, where PCBM is Phenyl-C61-butyric acid methyl ester and BCP is bathocuproine. We would like to note that SCLC is not a directly precise method for trap concentration measurement. There definitely might be a number of measurement errors related to the sample-to-sample variation or imprecisely measured film thickness, especially given that perovskite films are not completely smooth, so some natural thickness variation is always present. In our case we did our best to eliminate these errors by measuring perovskite's thickness at least 5 times for each perovskite and taking the average value. Similarly, we have measured

several SCLC devices for each system. Another major source of errors is the presence of Schottky barriers or other contact non-idealities in the device. They will significantly affect the I-V curve distorting the measured results. For this reason, we have used Mg layer with very low work function as injection electrode in the electron-only devices. Magnesium's low work function ensures Ohmic contact with n-type semiconductor. Additionally, for halide perovskites, ionic conductivity can play its role in the overall shape of the curve. We have employed pulsed SCLC measurements to minimize the impact of the ionic conductivity.

Suns-V_{OC} allowed us to calculate the ideality factor for each solution composition and demonstrated the highest ideality factor for pure DMF devices 1.45. AcN 1.2 M demonstrated ideality factor 1.29, NMP 0.72 M – similar 1.31 and DMSO 2.4 M – the lowest 1.21. SCLC revealed the values of electron trap density. DMSO 2.4 M demonstrated the lowest concentration of electron traps, which correlates well with the lowest ideality factor value.

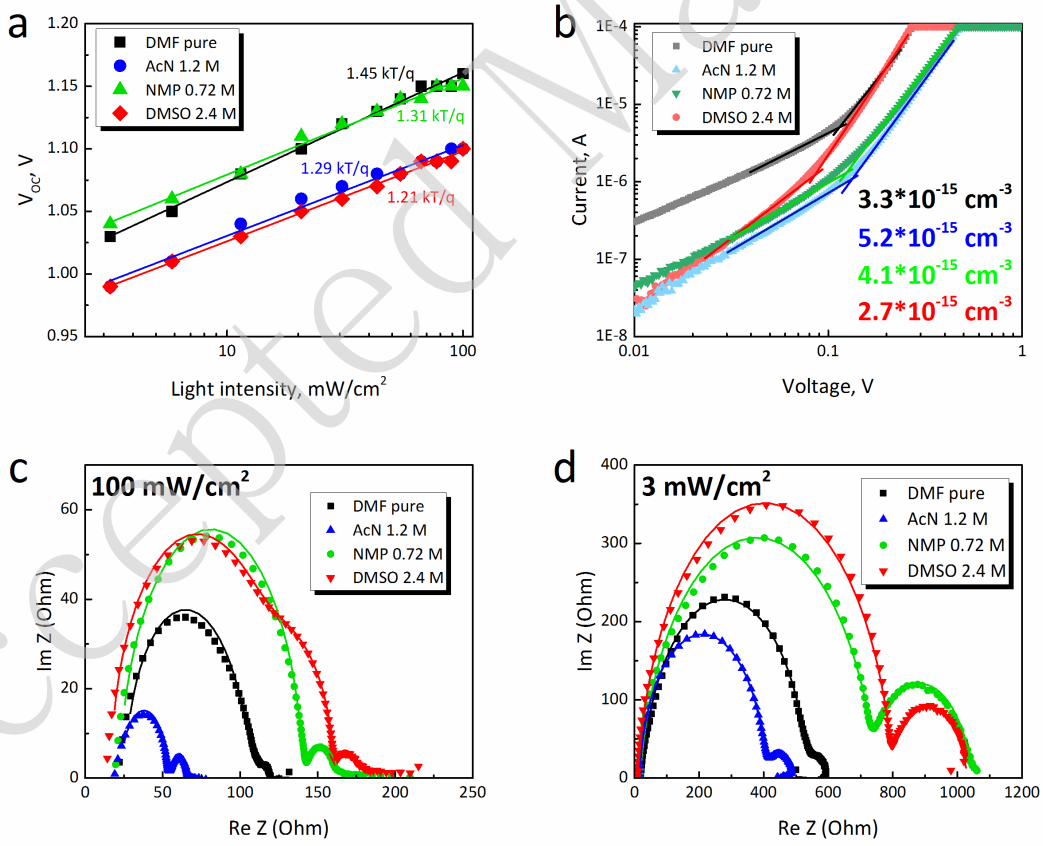

Figure 4. Suns-V_{OC} data for ITO/SnO_2/PCBA/perovskite/PTAA/VO_x/Al n-i-p solar cells based on four solvent compositions for perovskite layer (a). SCLC curves for electron-only devices ITO/SnO_2/PCBA/perovskite/PCBM/BCP/Mg/Al based on four solvent

compositions for perovskite layer with calculated concentration of electron traps (b). Impedance spectroscopy curves for ITO/SnO_2/PCBA/perovskite/PTAA/VO_x/Al n-i-p solar cells based on four solvent compositions for perovskite layer measured at 100 mW/cm^2 (c) and 3 mW/cm^2 (d).

Impedance spectroscopy (IS) was measured at two light intensities 100 mW/cm^2 (Fig. 4c) and 3 mW/cm^2 (Fig. 4d). We also measured dark IS before and after the *J*V measurement of the devices, the results are present in Supplement Fig. S6. Equivalent circuits used for curve fitting were taken from the Ref. 39 and are presented in Supplement Fig. S7. Calculated parameters are presented in Supplement Table 1-2. NMP 0.72 M and DMSO 2.4 M consistently show high recombination resistance at both light intensities. This means that their recombination rate is lower than in pure DMF and AcN 1.2 M devices. Interfacial trapping-related low-frequency capacitances C_{LF} are comparable in most cases: under 100 mW/cm^2 difference is negligible, while under 3 mW/cm^2 AcN has the highest C_{LF}, which correlates well with the highest trap density in SCLC. DMSO has mid-frequency semicircle at 100 mW/cm^2, definitely absent from all other systems and low-light DMSO spectrum. It means that at high carrier density transport layers extract charges slower than they are generated. For the dark IS measurement (Supplement, Fig. S6, Table 2) DMF and DMF:NMP-based samples show little change in parameters after the *J*V measurements. For DMF:NMP a small improvement can be seen by the increase of recombination resistance and decrease of charge transfer resistance. In contrast, DMF:DMSO and DMF:AcN systems feature notable drops in R_{LF} values which might point at slight increase in the interfacial trap density after light exposure. This is likely due to mobile ions that disrupt the interface under illumination. However, one should also note that these changes are still fairly small – about 10%.

Cross-sectional scanning electron microscopy was performed to obtain the images of the representative device cross-sections (Fig. 5). The pure DMF perovskite layer contains numerous inhomogeneities, which mostly disappear after the solvent modification. AcN 1.2 M film quality changes the most significantly: smooth surface, best among all the materials, constant non-defect thickness, grain boundaries become slightly visible. Similar effect was observed for NMP 0.72 M, but some intrinsic defects are still present in the perovskite film, especially on grain boundaries. DMSO 2.4 M perovskite film is homogeneous with clearly visible grain boundaries. It's also noticeable that the thickness of all bisolvent systems is higher than for pure DMF film,

and DMSO 2.4 M film has the highest, but not constant thickness.

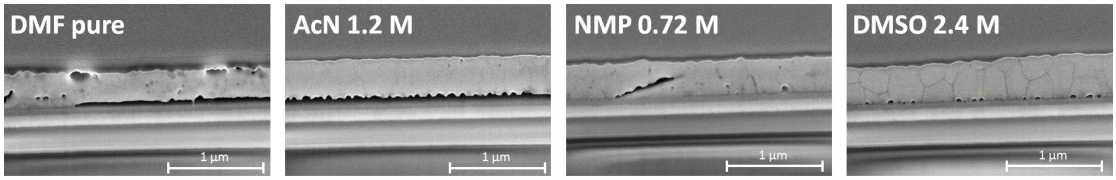

Figure 5. Cross-sectional SEM for ITO/SnO_2/PCBA/perovskite/PTAA/VO_x/Al n-i-p solar cells based on four solvent compositions for perovskite layer.

To understand the influence of additional solvents on perovskite material and device photostability, we proceeded with express test in inert atmosphere and simulated sunlight of 100 mW/cm^2 for solar cells and thin films on glass substrates covered with PTAA and VO_x layers. We observed the dynamics in film absorption (Fig. 6a) and normalized device PCE (Fig. 6b). Dynamics for all film UV-Vis spectra and solar cell parameters is presented in Supplement Fig. S8-S12.

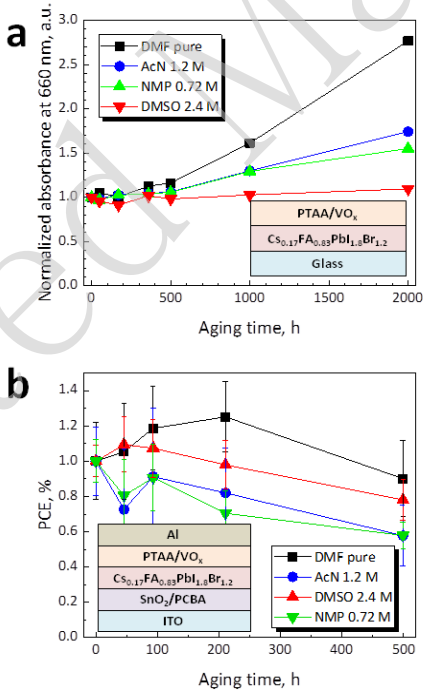

Figure 6. Normalized dynamics in UV-Vis spectra change at the wavelength 660 nm depending from the used additional solvent (a). Normalized dynamics in solar cell PCE change depending from the used additional solvent (a). Degradation conditions were 100 mW/cm^2 light intensity in inert conditions. Full UV-Vis spectra for all solvent concentrations can be found in Supplement Fig. S8-S11. Full un-normalized data for all device parameters can be found in Supplement Fig. S12.

Discussion

We identified the positive influence of all three used co-solvents AcN, NMP and DMSO on device parameters. It was noticeable, that all three solvents have various reasons behind the efficiency growth. Additional experiments conducted on perovskite thin films and full devices provided us with information necessary to make the following conclusions and assumptions.

Addition of 2.4 M DMSO (17.2 Vol%) leaded to the simultaneous increase in J_{SC} and FF (Fig. 1). Significant growth of current is mostly related to the "wrinkled" morphology and grain size growth, visible by SEM (Supplement, Fig. S3), Cross-sectional SEM (Fig. 5) and AFM (Fig. 3b). Improved quality and size of grains also leaded to the FF improvement. Increase in SSPL spectra indicates the growth in free charge carrier concentration. However, introduction of DMSO solvent leads to the strengthened interface recombination and appearance of injection barriers from the perovskite layer to the charge-transport layers. This can be confirmed by the slight decrease in device V_{OC} with DMSO addition and appearance of third semicircle on the impedance spectra measured at 100 mW/cm^2 as well as decrease of R_{LF} and increase of C_{LF} calculated from impedance spectroscopy (Supplement Table 1-2). We can also assume that the ideality factor of 1.21 which is closest to 1 among all solvents, in combination with low V_{OC} value indicates the dominance of interfacial Shockley-Read-Hall recombination.[35] This could happen due to the film morphology, since the following hole transport layer PTAA was deposited via spin-coating method, and resulting PTAA film quality and perovskite/PTAA interface can be disrupted by non-uniform deposition surface. It can also be partially related to the worsened adhesion of perovskite solution to the electron-transport layer, which was checked with contact angle technique (Supplement Fig. S13) with observed increase in contact angle value.

0.72 M on NMP (7 Vol%) enhanced the J_{SC} of the perovskite solar cells and very slightly increased the FF with almost no effect on V_{OC}. Usually the perovskite film thickness is the one responsible for the current density increase, but not in this particular case, since nor Cross-sectional-SEM, nor AFM, nor UV-Vis indicated any changes in perovskite thickness. Increase of charge carriers lifetime (Fig. 2c) and lower ideality factor (Fig. 4a) implied the slight improvement of perovskite film bulk quality, but cross-sectional SEM still demonstrated the presence of defects, mostly concentrated between the perovskite grains. And almost no changes

in C_{LF} and R_{LF} calculated from impedance spectroscopy indicated that addition of NMP does not deprave the interface between the perovskite and CTLs, unlike the addition of DMSO and AcN.

1.2 M concentration of AcN corresponding to the 8.6 Vol% leaded to the noticeable growth of solar cell FF from 60% to 67%. The FF of the solar cell mostly depends on the charge transport in all functional layers and charge extraction from perovskite into charge transport layers.[40] However, according to the device investigation by impedance spectroscopy and SCLC measurement (Fig. 4), the recombination rate and trap density for DMF:AcN devices only increases. So the main reason behind the improved FF and PCE of the device is drastically improved bulk film quality observed by AFM (Fig. 3b) and cross-sectional SEM (Fig. 5), which also affects the charge transport in the perovskite layer because of reduced series resistance. This effect was proved by TRPL conducted for perovskite films (Fig. 2c) and ideality factor (Fig. 4a). The problem still lays within the interface between the perovskite and CTLs. Since the morphology of the film was the best among the four and the adhesion of AcN 1.2 M perovskite solution was the best among all compositions according to the contact angle (Supplement Fig. S13) we can make a hypothesis that some carrier traps can accumulate on the interface between the perovskite and CTLs. The nature of this traps should be investigated by more advanced methods and there is a high possibility that a direct passivation approach could further improve the DMF-AcN processed perovskite material.

There are obvious solvent properties that always influence the film formation process strongly, such as density (DMF - 0.94 g/cm^3, AcN - 0.79 g/cm^3, NMP 1.03 g/cm^3, DMSO - 1.1 g/cm^3) and dynamic viscosity (DMF - 0.92 mPa·s, AcN - 0.35 mPa·s, NMP 1.65 mPa·s, DMSO - 1.996 mPa·s). High dynamic viscosity of DMSO might be the reason behind the worsened adhesion of DMF:DMSO solution to the ETL, but simultaneously it influences the grain formation and, as expected, their size and film morphology. But this won't be the same for AcN solvent, which has lower density and viscosity than DMF. Another important parameter is boiling temperature of the solvent (DMF - 153°C, AcN - 82°C, NMP - 202°C, DMSO - 189°C). Slower evaporation of high boiling point solvents like DMSO and NMP might induce slower crystallization which favors the growth of larger grains. Indeed, our AFM data supports this assumption (Supplement Table 4). After the solution deposition and antisolvent application we heat up samples to ensure the grain growth and evaporation of the remaining solvents. And since we heat up our films up to 100-120°C, then there is high

probability, that some amount of DMF, DMSO and NMP molecules will remain in the perovskite film. The influence of the remaining solvent molecules can be both positive, if they are concentrated on grain boundaries providing surface trap passivation, or negative, if they are concentrated in the bulk where they can produce impurity states within the bandgap. And the probability for AcN molecules to remain in the film will be much lower because of its low boiling temperature. Finally, all our solvents have a dipole moment (DMF - 3.82, AcN - 3.92, NMP - 4.09, DMSO 3.96), which influences the lead coordination in the mixture solution, the higher the dipole moment — higher the coordination capacity of a solvent. However, the values of dipole moments are fairly close, therefore, we don't expect any considerable influence from this factor.

Photoinduced degradation of perovskite films covered with PTAA/VO_x revealed the positive effect of binary solvents on stability, which is unsurprising since all three additional solvents improved the bulk perovskite film (Fig. 6). The best stability was observed for DMSO 2.4 M films. Overall, all systems demonstrated rapid degradation of films, which is most likely related to the phase segregation. On some of UV-Vis spectra the formation of a perovskite shoulder close to 800 nm can be observed, which corresponds to the formation of the new phase (Supplement Fig. S9-11). Surprisingly, when we switched to the device photoinduced degradation, the most stable solar cells were ones with pure DMF based perovskite. However, this effect is deceptive, since the efficiency increases in the beginning of the process for pure DMF system, which is also related to the phase segregation and formation of narrow-bandgap phase. Binary solvent systems did not demonstrate such increase in efficiency from the start. But still, the degradation of all perovskite solar cells is most likely related to the phase segregation. We also would like to point out the necessity to improve the interfaces of perovskite/CTLs according to our previous assumptions that addition of both DMSO and AcN in perovskite solution negatively influences the interface quality in solar cell, while improving the bulk. The development of the suitable CTLs for WBG perovskite materials is necessary to ensure their stability and improve device parameters, since the SnO_2 and PTAA energy levels align well with $MAPbI_3$ and other materials with bandgap close to 1.5-1.6 eV, but poorly align with wide bandgap materials (1.75 eV and higher). This was also the reason behind the reduced V_{OC} parameters of our devices.

Finally, we decided also check the influence of additional solvent on the fabrication of perovskite mini-modules. 25 cm^2 total size mini-modules with work-area 16 cm^2,

effective area 13.2 cm^2 (GFF = 82.5%) consisting of total 6 sequentially connected cells 2.2 cm^2 were produced with the methodic nearly identical to the previously made laboratory devices. J-V curves of the typical representatives of every solvent configuration are presented on Fig. 7, the PCE highlighted near each curve of the mini-modules was calculated for the effective area of 13.2 cm^2. MPPT of the devices is presented in Supplement, Fig. S14. And here we can unexpectedly observe that the best device parameters were demonstrated by AcN 1.2 M processed devices. For such devices we were able to obtain modules with efficiency 9.7% with the highest V_{OC} and FF among all modules. Second was the pure DMF based modules, which also demonstrated good V_{OC} and FF. At the same time we weren't able to obtain good modules with DMF:DMSO and DMF:NMP based perovskites via spin-coating method. Low efficiency of such devices related mostly to the much lower FF and V_{OC} which points to the high defectiveness of the films. In case of DMSO modules this effect is most likely related to the "wrinkled" morphology and related difficulties of spin-coated deposition of PTAA layer on top of it. NMP mini-module low performance is most likely related to the poor quality of the perovskite bulk film, which is enhanced when upscaled. Thus, the most suitable perovskite processing method for large-area devices is based on DMF:AcN solution of perovskite. To check our assumption, we performed the photoluminescence mapping of the spincoated perovskite films on 5x5 cm glass substrates (Suplement Fig. S15). PL mapping confirmed that pure DMF films had some amount of rotation-caused stripes and defects. For NMP 0.72 M number of visible defects increased and overall uniformity of the film was disturbed. DMSO 2.4 M films demonstrated uneven PL because of morphology, and with the measurement moving from left to right, the intensity of the PL increased, which pointed out the progressing film degradation during measurement under the green laser exposure. And AcN 1.2 M films demonstrated the brightest PL response, quite uniform through the film workarea.

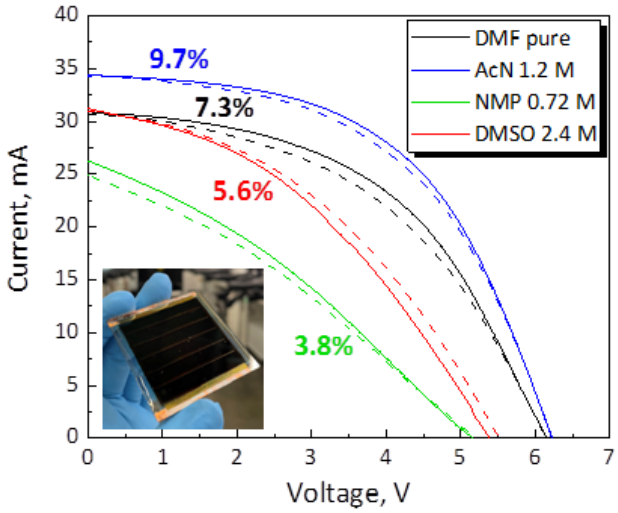

Figure 7. J-V curves for perovskite mini-modules of total size 25 cm^2 with effective area 13.2 cm^2 consisting of total 6 sequentially connected cells 2.2 cm^2

In conclusion, we improved the device characteristics, stability and suitability for large-scale processing. We utilized conventional perovskite solvent DMF and three additional solvents DMSO, NMP and AcN. It was revealed that implementing of all three leads to the increase of laboratory device efficiency, but the necessary concentration is unique for every solvent. We also were able to assume various processes behind the improvement mechanisms. DMSO addition improves overall quality of the film, increases the perovskite grain size and thickness while producing the "wrinkled" surface. Improved film quality leads to the growth in free charge carrier concentration. However, simultaneously the interface between the perovskite and CTL suffers from the increased interface recombination and worsened adhesion to the HTL. NMP is the solvent with the least visible effects on perovskite film quality, since some defects are still present in the film. However, unlike DMSO, it doesn't impair the CTL-perovskite interfaces. And implementation of AcN gave unwittingly interesting results. It significantly improved the bulk film quality, morphology and adhesion to ETL, but carrier traps were presumably the cause of low efficiency. However, this solvent demonstrated the best predisposition for upscailing, allowing us to produce 25 cm^2 modules with efficiency 9.7%. We also assume that problems with interface are related to the carrier traps accumulation. So the further improvement of such material is possible with advanced analysis of the carrier traps nature and appropriate passivation approach. We also would like to point out the further necessity to find the best CTLs

(especially ETL) for this perovskite to ensure its stability and increase efficiency.

Materials and Methods

Materials Cesium iodide (CsI, 99.9%), lead (II) bromide ($PbBr_2$, ≥ 98%), poly[bis(4-phenyl)(2,4,6-trimethylphenyl)amine (PTAA) and vanadium (V) oxide (V_2O_5, 99.95%) were purchased from Sigma-Aldrich. Other materials were purchased from different companies: lead (II) iodide (PbI_2, Chem synthesis), tin (IV) oxide nanoparticles (SnO_2, 15% in H_2O colloidal dispersion, Alfa Aesar).

Formamidinium iodide ($(NH_2CH=NH_2)I$ or FAI) was synthesized by the procedure described in Ref. 41; 6,6-phenyl-C61 butyric acid (PCBA) was synthesized by the procedure described in Ref. 42.

Sample fabrication The $Cs_{0.17}FA_{0.83}PbI_{1.8}Br_{1.2}$ solution was prepared by mixing CsI, FAI, $PbBr_2$, PbI_2 in a corresponding stoichiometry ratios. The mixed powders were then fully dissolved in DMF to get 1.5 M mother liquor. To obtain required binary solvent systems a mother liquor was diluted by the corresponding amount of DMF-X mixture (X = DMSO, NMP, AcN) so that the final concentration of perovskite would be 1.2 M. For instance, to make 1 ml of 1.2 M DMSO solution, 114 µl of DMF and 86 µl of DMSO would be added to the 800 µl of mother liquor. The solutions would be left overnight before spin-coating.

Thin films of perovskite were prepared by spin-coating deposition method at the 3000 rpm followed by ethyl acetate anti-solvent deposition. Then all films were heated for 10 min at 120℃ for DMF:DMSO films and 100℃ for all other solvents. The entire process was performed in a N_2 glovebox (H_2O < 0.1 ppm and O_2 < 0.1 ppm).

For n-i-p solar cell preparation, the ITO substrates were sequentially cleaned via sonication in deionized water, acetone and isopropanol followed by a 10 min air plasma treatment. To form the ETL a 10% SnO_2 solution was deposited by spin-coating in ambient conditions at 5000 rpm and annealed at 175℃ for 30 min. After that the substrates were transferred to a N_2 glovebox, where all the following manipulations were performed. The substrates were annealed at 150℃ for 10 min. After that 0.2 mg/ml PCBA (Phenyl-C61-butyric Acid) solution in chlorobenzene was applied by spin-coater at 3000 rpm and annealed at 100℃ for 10 min. After that the

perovskite layer was deposited as described above. Then to make the hole-transport layer (HTL), firstly hot (75-80℃) PTAA (poly[bis(4-phenyl)(2,4,6-trimethylphenyl)amine) solution (15 mg/ml in chlorobenzene) was deposited on a spinning substrate at 4000 rpm. Thermal evaporation was then used to deposit 30 nm of VO_x and either 150 nm of Al (for regular devices) or 120 nm of Ag (for the devices used for the EQE measurement).

For mini-module processing we performed photoresist etching of ITO to get a specific pattern for transparent electrodes (P1 line). Then SnO_2, PCBA, perovskite, PTAA and VO_x layers were deposited with the same processing methods as for laboratory devices. Then we created the P2 line over all deposited layers by mechanical scratching with a scalpel and deposited 150 nm of Al as top electrodes through the shadow mask to ensure the P3 line.

Sample characterization

The devices were tested using an AM 1.5G simulator (Newport Verasol AAA solar simulator and Advantest 6240 A source-measurement units) in a N_2 glovebox.

External quantum efficiency (EQE) measurements were performed utilizing a Newport Oriel IQE200 with chopped light at a frequency of 72 Hz.

X-ray Diffraction (XRD) of the perovskite films was measured on air with an X-ray diffractometer Bruker D8 Advance with CuKα X-ray source and LYNXEYE XY detector, under the θ/2θ mode with 40 kV and 200 mA power conditions.

Steady-state PL and PL mapping experiments were performed on custom LBIC+PL+EL microscopy setup from an Automatic Research GmbH with a Horiba spectrometer. Excitation was done by a 2.5 μW power 535 nm laser.

Absorbance spectra of the perovskite films in the UV-visible region were measured using an Avantes AvaSpec-HS2048 dual-channel optical spectrometer.

Time-resolved PL measurements was performed with time correlated single photon counter (TCSPC) technique on Horiba QuantaMaster spectrofluorometer. Peak emission was set up to 730 nm, entrance slit 5 nm, time range 1.6 μs, 1000 counts for peak channel. Excitation power density – 2.54 nJ/cm^2 and the excitation source – diDiode 345 nm. The excitation source was first going through the perovskite material and then through the substrate glass, that excludes the impact of gamma-ray-induced

substrate darkening.

The morphology of the perovskite films was characterized using an atomic force microscope (AFM) (NANOEDUCATOR, NT-MDT, Moscow, Russia). The film thickness was measured using AFM microscopy while scanning a thin scratch on the top of the films.

The SEM and Cross-SEM images were obtained on Dual beam scanning electron microscope Helios G4 Plasma FIB UXe. TLD detector, Probe current 25 pA, Landing voltage 5 kV. To study the multilayer structure of sample in the region of interest, a cross-section was performed with an ion beam. To create a cross-section in the region of interest, a protective layer of platinum was deposited using the gas injection method. The area of interest with protective layer of platinum was milled by ion beam, followed by visualization of the cross-section with an electron beam. The assigned images were programmatically reconstructed taking into account the angle between the cross-section surface and the electron beam.

Stability tests

For the stability test the perovskite films were applied on glass substrates and covered with PTAA and VO_x according to the procedure described in perovskite solar cell fabrication section. The operational stability tests were carried out in a N_2 glovebox under simulated AM 1.5G illumination (100 mW/cm^2, Class AAA multi-color LED solar simulator, Guangzhou Crysco Equipment Co. Ltd). Absorbance spectra were measured before exposure to sun light and during the stability test, relative change in absorbance of 660 nm wavelength light was plotted to visualize the degradation process occurring in the films.

Acknowledgements

This work was supported by Russian Science Foundation (project No. 23-72-01114). The synthesis of FAI was funded by the Ministry of Science and Higher Education of the Russian Federation (project 122111700041-8).

Author Contributions

O. R. Parfenova supervised the whole project and prepared mini-modules samples. S. A. Djouse-Ivanina carried out the optimization and sample preparation, measurement of perovskite film optical and structural characteristics. A. V. Novikov measured the

SCLC, Impedance Spectroscopy and Suns-V_{OC}. P. Griscenco carried out the degradation experiments. I. N. Krupatin carried out the cross-sectional SEM measurement and analysis. M. M. Tepliakova carried out the experiments related to the TRPL. I. E. Kuznetsov and A. V. Akkuratov carried out the synthesis of the organic materials used in this work. S. Yu. Luchkin carried out the experiments and data analysis of AFM. All authors participated in the analysis of data and contributed to the writing of manuscript.

Conflict of interest

The authors declare no competing interests.

Supplementary information

Supplementary materials are available at the online version.

References(Reference 40 is not cited in the main text, please check)

1. Kojima, A. et al. Organometal halide perovskites as visible-light sensitizers for photovoltaic cells. *Journal of the American Chemical Society* **131**, 6050-6051 (2009).

2. Park, J. et al. Controlled growth of perovskite layers with volatile alkylammonium chlorides. *Nature* **616**, 724-730 (2023).

3. Polyzoidis, C., Rogdakis, K. & Kymakis, E. Indoor perovskite photovoltaics for the internet of things—challenges and opportunities toward market uptake. *Advanced Energy Materials* **11**, 2101854 (2021).

4. Wojciechowski, K., Forgács, D. & Rivera, T. Industrial opportunities and challenges for perovskite photovoltaic technology. *Solar RRL* **3**, 1900144 (2019).

5. Martulli, A. et al. Towards market commercialization: lifecycle economic and environmental evaluation of scalable perovskite solar cells. *Progress in Photovoltaics: Research and Applications* **31**, 180-194 (2023).

6. Barker, A. J. et al. Defect-assisted photoinduced halide segregation in mixed-halide perovskite thin films. *ACS Energy Letters* **2**, 1416-1424 (2017).

7. Chen, S. et al. Exploring the stability of novel wide bandgap perovskites by a robot based high throughput approach. *Advanced Energy Materials* **8**, 1701543 (2018).

8. Li, Z. et al. Minimized surface deficiency on wide-bandgap perovskite for efficient indoor photovoltaics. *Nano Energy* **78**, 105377 (2020).

9. Chen, C. et al. Arylammonium-assisted reduction of the open-circuit voltage deficit in wide-bandgap perovskite solar cells: the role of suppressed ion migration. *ACS Energy Letters* **5**, 2560-2568 (2020).

10. Correa-Baena, J. P. et al. The rapid evolution of highly efficient perovskite solar cells. *Energy & Environmental Science* **10**, 710-727 (2017).

11. Rehman, W. et al. Charge-carrier dynamics and mobilities in formamidinium lead mixed-halide perovskites. *Advanced Materials* **27**, 7938-7944 (2015).

12. Rehman, W. et al. Photovoltaic mixed-cation lead mixed-halide perovskites: links between crystallinity, photo-stability and electronic properties. *Energy & Environmental Science* **10**, 361-369 (2017).

13. Bush, K. A. et al. Compositional engineering for efficient wide band gap perovskites with improved stability to photoinduced phase segregation. *ACS Energy Letters* **3**, 428-435 (2018).

14. Xu, F. et al. Challenges and perspectives toward future wide-bandgap mixed-halide perovskite photovoltaics. *Advanced Energy Materials* **13**, 2203911 (2023).

15. Saliba, M. et al. Perovskite solar cells: from the atomic level to film quality and device performance. *Angewandte Chemie International Edition* **57**, 2554-2569 (2018).

16. Xu, J. X. et al. Triple-halide wide-band gap perovskites with suppressed phase segregation for efficient tandems. *Science* **367**, 1097-1104 (2020).

17. Wen, J. et al. Steric engineering enables efficient and photostable wide-bandgap perovskites for all-perovskite tandem solar cells. *Advanced*

Materials **34**, 2110356 (2022).

18. Zhou, Y. et al. Benzylamine-treated wide-bandgap perovskite with high thermal-photostability and photovoltaic performance. *Advanced Energy Materials* **7**, 1701048 (2017).

19. Wang, C. et al. Suppressing phase segregation in wide bandgap perovskites for monolithic perovskite/organic tandem solar cells with reduced voltage loss. *Small* **18**, 2204081 (2022).

20. Liang, J. W. et al. Suppressing the phase segregation with potassium for highly efficient and photostable inverted wide-band gap halide perovskite solar cells. *ACS Applied Materials & Interfaces* **12**, 48458-48466 (2020).

21. Li, G. et al. Co-solvent engineering contributing to achieve high-performance perovskite solar cells and modules based on anti-solvent free technology. *Small* **19**, 2301323 (2023).

22. Han, E. Q. et al. High-performance indoor perovskite solar cells by self-suppression of intrinsic defects via a facile solvent-engineering strategy. *Small* **20**, 2305192 (2024).

23. Han, Y. P. et al. Review of two-step method for lead halide perovskite solar cells. *Solar RRL* **6**, 2101007 (2022).

24. Wang, Z. Y. et al. Antisolvent- and annealing-free deposition for highly stable efficient perovskite solar cells via modified ZnO. *Advanced Science* **8**, 2002860 (2021).

25. Lohmann, K. B. et al. Solvent-free method for defect reduction and improved performance of p-i-n vapor-deposited perovskite solar cells. *ACS Energy Letters* **7**, 1903-1911 (2022).

26. Cai, B., Zhang, W. H. & Qiu, J. S. Solvent engineering of spin-coating solutions for planar-structured high-efficiency perovskite solar cells. *Chinese Journal of Catalysis* **36**, 1183-1190 (2015).

27. Liu, Y. W. et al. Solvent engineering of perovskite crystallization for high band gap $FAPbBr_3$ perovskite solar cells prepared in ambient condition. *ACS*

Applied Energy Materials **6**, 7102-7108 (2023).

28. Lee, J. W. et al. Tuning molecular interactions for highly reproducible and efficient formamidinium perovskite solar cells via adduct approach. *Journal of the American Chemical Society* **140**, 6317-6324 (2018).

29. Chen, H. Q. et al. Solvent engineering for high-performance two-dimensional ruddlesden-popper $CsPbI_3$ solar cells. *ACS Applied Energy Materials* **5**, 11807-11814 (2022).

30. Li, Y. Y. et al. Solvent modification to suppress halide segregation in mixed halide perovskite solar cells. *Journal of Materials Science* **55**, 9787-9794 (2020).

31. McMeekin, D. P. et al. A mixed-cation lead mixed-halide perovskite absorber for tandem solar cells. *Science* **351**, 151-155 (2016).

32. Zhou, Y. et al. Composition-tuned wide bandgap perovskites: from grain engineering to stability and performance improvement. *Advanced Functional Materials* **28**, 1803130 (2018).

33. Oliver, R. D. J. et al. Understanding and suppressing non-radiative losses in methylammonium-free wide-bandgap perovskite solar cells. *Energy & Environmental Science* **15**, 714-726 (2022).

34. Yu, F. et al. Efficient and stable wide-bandgap perovskite solar cells derived from a thermodynamic phase-pure intermediate. *Solar RRL* **6**, 2100906 (2022).

35. Li, C. et al. Emission enhancement and intermittency in polycrystalline organolead halide perovskite films. *Molecules* **21**, 1081 (2016).

36. Chen, J. et al. Carrier dynamic process in all-inorganic halide perovskites explored by photoluminescence spectra. *Photonics Research* **9**, 151-170 (2021).

37. Péan, E. V. et al. Interpreting time-resolved photoluminescence of perovskite materials. *Physical Chemistry Chemical Physics* **22**, 28345-28358 (2020).

38. Kim, J. B. et al. Wrinkles and deep folds as photonic structures in photovoltaics. *Nature Photonics* **6**, 327-332 (2012).

39. Guerrero, A. et al. Properties of contact and bulk impedances in hybrid lead halide perovskite solar cells including inductive loop elements. *The Journal of Physical Chemistry C* **120**, 8023-8032 (2016).

40. These, A. et al. Beginner's guide to visual analysis of perovskite and organic solar cell current density-voltage characteristics. *Advanced Energy Materials* **14**, 2400055 (2024).

41. Eperon, G. E. et al. Formamidinium lead trihalide: a broadly tunable perovskite for efficient planar heterojunction solar cells. *Energy & Environmental Science* **7**, 982-988 (2014).

42. Hummelen, J. C. et al. Preparation and characterization of fulleroid and methanofullerene derivatives. *The Journal of Organic Chemistry* **60**, 532-538 (1995).